THE PUBLISHING HOUSE
OF THE ROMANIAN ACADEMY

PROCEEDINGS OF THE ROMANIAN ACADEMY, Series A,
Volume 13, Number 2/2012, pp. 125–132

LOW-SPEED-SMALL-LOAD DIRECT TORQUE CONTROL RIPPLES FILTERING

Ion Rares STANCIU[*], Gheorghita GINGA[*], Sebastian MUNTEAN[**], Liviu Eugen ANTON[*]

[*] "Politehnica" University of Timisoara
[**] Romanian Academy, Timisoara Branch
E-mail: rares.stanciu@mh.mec.upt.ro

A viable alternative for electricity production is hydroelectricity. Certain advantages as being renewable, having the lowest price/KWh and the possibility of regulating the power grid recommends hydroelectricity today. However, the power-plants are aging. Simulation and experimental testing work hand in hand to ensure increase their efficiency. Testing is considered to be complete if performed at multiple speed values. Low-speed-small-load test reveals the presence of noise generated by torque ripples. Adding a speed sensor would eliminate this noise. This paper presents a method which eliminates the low-speed noise while preserving the sensorless advantage.

Key words: direct torque control, induction motors, Kalman filters.

1. INTRODUCTION

As the society evolve, the demand for electrical energy increases. The population has grown and it shall continue to grow. Large, comfortable, temperature-controlled homes, fast and luxurious means of transportation, an increasing number of electrically-operated tools, they all need electricity to operate.

When (re)designing hydraulic machines, a scaled-down model is built for testing purpose. Equivalence equations are used to transpose parameter values from the machine to the model and vice versa. Experiments are performed to assess the hydro-machine's behavior from energetic and cavitational point of view (testing has two important directions). Energetically, the characteristic of head, mechanical power and efficiency are important. A second set of characteristics targets the machine behavior in case of cavitation. Testing is also used by researchers to validate their numerical results [3] or fault diagnosis [13]. Experiments at different flow rates were performed in [10] to investigate the slip factor of centrifugal pumps and at different flow rates.

Testing is considered to be complete if it is done at several different speed values. It is important to note that speed has to be constant during the experiments. In case of speed-dependant loads, a closed-control loop has to exist to ensure a constant speed. Examples of speed-dependant loads include fans and pumps.

Induction motors are the industry's workhorse today. Together with the constructive simplicity, the absence of brushes and the low-cost maintenance make the induction motor the preferred actuator. Its single drawback is related to speed adjustment. The most convenient speed adjustment method (from energetic point of view) powers the motor with variable frequency. Equation 1 relates the power frequency to the speed of the rotating magnetic field in the motor.

$$f = p \cdot n. \tag{1}$$

Here, the constant p is a constructive motor parameter. In case of induction motor, the rotor follows the magnetic field with a slightly smaller speed. When reducing the AC frequency, one has to decrease the voltage to avoid damaging the motor. This method is called the $V/f = \text{const.}$ A frequency converter (oftentimes called inverter) is used to deliver variable frequency AC power to the motor (Fig. 1). It uses six transistors to convert the DC power to AC. However, the $V/f = \text{const.}$ method has certain limitations. For small speed and small loads it generates prohibitive torque pulsations.

To sidestep this Field Oriented technologies were developed. Among them, the Direct Torque Control (DTC) has been generally accepted almost as a new standard. The DTC provides very good dynamic response and has the advantage of a simple implementation. Its "sensorless" capability combined with a closed-loop speed control satisfies a significant percentage of real-life applications.

If actuating speed-dependant loads (for example a pump) at low speed values, the sensorless DTC solution reveals torque pulsations which propagates in the speed-plot, mechanical power plot, etc. If this data is used (speed, mechanical power, etc.) to compute other variables (the efficiency for example), the ripples will affect them as well. Different techniques have been proposed to eliminate torque ripples while preserving the "sensorless" advantage. Lascu et al [8] introduced a modified direct torque and flux control based on the space vector modulation (DTC-SVM). Using an improved voltage-current model speed observer, this technique considerably reduces the torque and speed pulsations during the steady state operation. Beerten et al [4] proposed a predictive technique which reduces torque ripples generated by the time delays associated with data processing. Taking advantage of a low computation complexity, this method can be extended to compensate for time delays. Zidani and Said [17] introduced fuzzy to minimize the torque ripples. These control techniques successfully reduce torque ripples but, they target the inverter control only and assume access to its microprocessor. This paper presents a method to eliminate the torque ripple of a DTC inverter. It preserves the DTC advantages (simplicity, sensorless actuation, etc.) and uses software implemented filters. Section 2 briefly discusses the DTC technology. After describing our hardware, Section 3 presents the theory behind the selected filter. Its implementation together with experiments and results are described in Section 4. Section 5 discuses conclusions and future work.

2. THE DIRECT TORQUE CONTROL TECHNOLOGY

The development of the Field Oriented Control technologies was a big step forward because it meant a tremendous increase in the induction motor's performance. A new concept proposed in the 80s and called the Direct Torque Control (DTC) was widely accepted. This technology was developed by several researchers ([5, 6, 14]). Introduced by ABB, this technology is not restricted to the induction motor. The DTC does not require coordinate transformations or modulation blocks [15].

The standard DTC makes use of two hysteresis comparators for torque and flux (Fig. 3). These comparators limit the flux and torque to their thresholds. Consequently, the switching frequency is not constant.

Assuming a voltage V that powers the inverter and denoting the upper switches as T_a, T_b, T_c ($T_k = 1$ means switch on while 0 means off; the lower switches are always in opposite state to avoid short-circuits) the voltages applied to the motor are given by equations 2.

$$\begin{aligned} v_{as} &= \frac{2T_a - T_b - T_c}{3} \cdot V, \\ v_{bs} &= \frac{-T_a + 2T_b - T_c}{3} \cdot V, \\ v_{cs} &= \frac{-T_a - T_b + 2T_c}{3} \cdot V, \end{aligned} \tag{2}$$

$$\overline{v_s} = \frac{2}{3} \cdot V \left(T_a + T_b \cdot \mathrm{e}^{\mathrm{j} \cdot \frac{2\pi}{3}} + T_c \cdot \mathrm{e}^{\mathrm{j} \cdot \frac{4\pi}{3}} \right). \tag{3}$$

Using an inverter to power the motor (Fig. 1), the DTC technology (Fig. 2) focuses on induction motor flux and torque producing capabilities. A closed loop estimator is used to calculate the stator flux and torque using the stator variables. There are three phases and eight possible states of the inverter (Fig. 1). The voltage vector is formed according to equation 3 and may take 8 values (six non-zero values and two zero values).

The six possible values can be seen in Fig. 2. The other two represent the cases when all switches are either 1 or 0. In both these cases the generated voltage vector is zero.

An important module in the inverter is the flux and torque estimator (Fig. 3). It estimates the magnetic flux and its orientation. The flux may be computed by integrating the difference between the applied voltage and the voltage drop. Equations 4 can be used to estimate the $d-q$ flux components. Consequently, the magnitude of the stator flux is given by equation 5. The motor's torque is computed using equation 6. The estimated values for both variables are compared with the reference and error signals are computed. These error signals are fed to the hysteresis comparators which establish if the torque/flux should increase/decrease (Fig. 2). This information is passed to the Switching Table (Fig. 3), which decides which vector has to be applied to the motor.

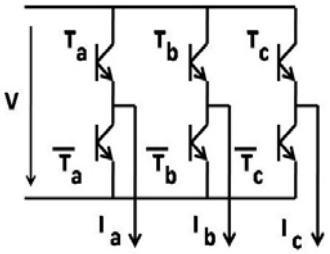

Fig. 1 – The schematic of an inverter.

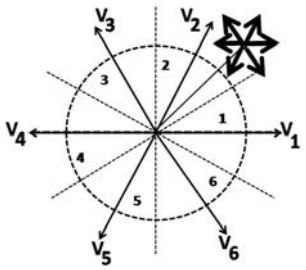

Fig. 2 – The six voltage vectors and the six sectors partitions.

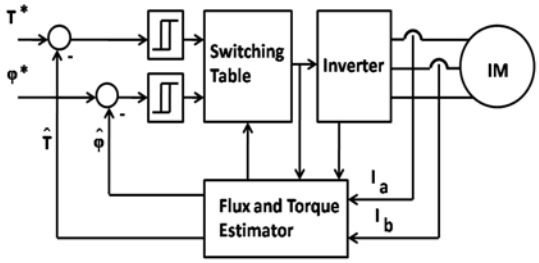

Fig. 3 – The schematic block diagram of the Direct Torque Control technology.

Assuming the flux vector located in the second sector (Fig. 2), all six voltage vectors can be applied to the motor. For a counter-clockwise rotation a V_2 application would increase both the flux and the torque. Appling a V_4 vector has the effect of increasing the torque and decreasing the flux. Applying the V_1 vector would increase the flux and reduce the torque while a V_5 has the effect of reducing both of them. This approach allows the inverter to control both the flux and the torque in the motor.

$$\begin{aligned}\overline{\varphi_{sd}} &= \int_0^t \left(\overline{v_{sd}} - R_s \cdot \overline{I_{sd}}\right) \cdot \mathrm{d}t, \\ \overline{\varphi_{sq}} &= \int_0^t \left(\overline{v_{sq}} - R_s \cdot \overline{I_{sq}}\right) \cdot \mathrm{d}t.\end{aligned} \tag{4}$$

As mentioned above, when actuating speed-dependant loads at low speed using DTC standard, torque ripples occur.

$$\varphi_s = \sqrt{\varphi_{sd}^2 + \varphi_{sq}^2}, \tag{5}$$

$$T_e = p \cdot \left(\varphi_{sd} \cdot I_{sq} - \varphi_{sq} \cdot I_{sd}\right). \tag{6}$$

3. FILTERING THE DATA

3.1. The testing rig

The low-speed torque ripples (which translated into speed and mechanical power pulsations) were detected experimentally. A test rig was built in the Pumps Laboratory at "Politehnica" University of Timisoara. Destined to cover the hydro-units experimental testing, the rig was a team effort. It is composed of a closed hydraulic circuit (denoted by 5, 8, 10-12, 14, 15 in Fig. 4 left), two reservoirs of $1\mathrm{m}^3$ each (denoted by 1 in Fig. 4 left), vanes (denoted by 4, 9, and 16 in Fig. 4 left), a PCN 80-200 pump, a 37kW

induction motor, power electronics, sensors (for pressure, temperature, discharge and electrical power), and data acquisition system to acquire sensors data. For testing purpose, the goal is to acquire the inlet and outlet pressure, the discharge, the temperature, the speed, the mechanical and the electrical power. The inlet and outlet pipes diameters are 0.1m and 0.08m, respectively. The pressure sensors height with respect to the pump are $Z_{asp} = 0.01$m and $Z_{ref} = 0.75$m (see Fig. 4 right).

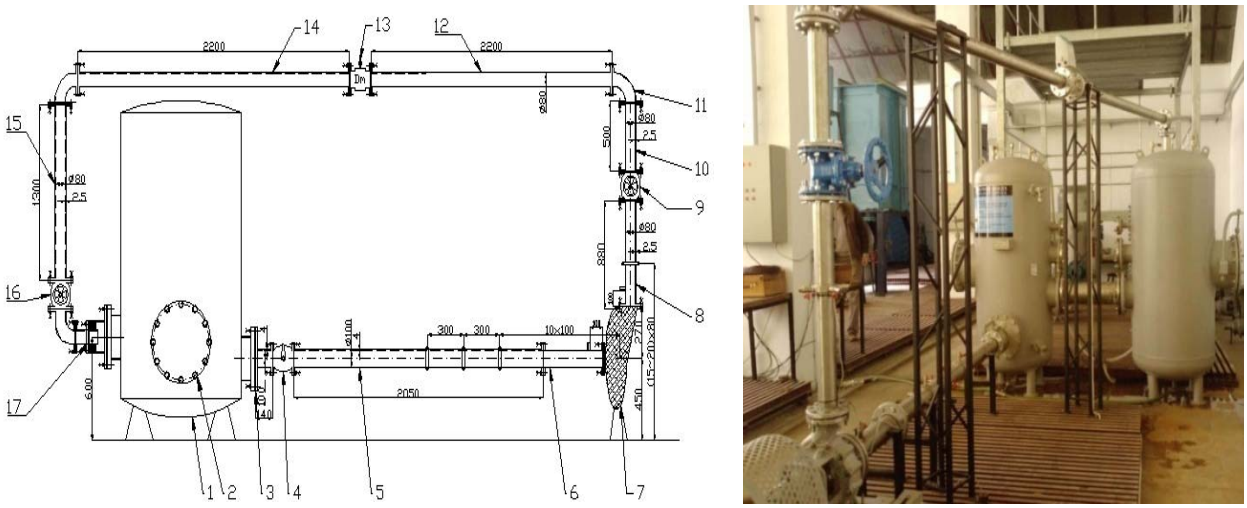

Fig. 4 – The test rig: schematic (left) and picture (right).

An acquisition system was built to acquire the inlet and outlet pressures, the speed, the discharge, the electrical power and the fluid temperature. Called "SES-A1" and built as a distinct module, it has 32 channels (with voltage/current differential inputs), 12 bits resolution, 100kb/sec acquisition frequency, 512k sample memory and allows computer connection. The Electronic Interface module provides the compatibility needed for computer interfacing using the RS232 standard. A block diagram of the acquisition system can be seen in Fig. 5. Aside from powering the motor, the inverter is also used to acquire the electrical power, the mechanical power and the speed.

The SES-A1 board is able to accommodate the voltage-output or the current-output sensors. Several sensors are used to convert the pressure, flow, and temperature into electric signals. They are directly interfaced with the data acquisition system. The inlet pressure sensor's pressure range is –1÷2.5bar with an output current in the range of 4÷20 mA. Its accuracy reported to be ±0.25%. The outlet pressure sensor's input pressure range is 0÷6 bar with an output is a current in the range of 4÷20 mA. The accuracy reported by the manufacturer is ± 0.25%. An electromagnetic flow meter is used to measure the discharge. Its domain is in 0÷50 l/s range and its precision is reported to be 0.4%. For an accurate measurement the electromagnetic flow meter has to be completely filled with water. Consequently, this device was installed on the rig's top pipe.

A software platform was needed in order to control the rig using a computer. This platform acquires the variables (the motor's speed, the temperature, the inlet and outlet pressures, and the discharge) and stores them into a file. It has the real-time plotting capability and the possibility of performing calculations. Its Graphical User Interface (GUI) displays the instantaneous values received from the SES-A1. It also contains a graphical area which plots the curve $H = f(Q)$. The software platform was developed in Visual Studio 2008 in C#.

For testing purpose, speed-adjustment is important. To be able to modify the speed the inverter-induction motor solution was chosen. To ensure a large speed range adjustment (500 rpm–3 000 rpm) and low torque pulsations, the DTC technology was preferred. A 45kW-DTC-inverter was installed to actuate the rig's motor at variable speed. Its advantages are: sensorless solution, wide range variable speed, computer controllable, etc. For these inverters, the reported torque response is 1–2 ms below 40 Hz while the sensorless speed accuracy is 10%. If using a 1 024 pulses/revolution encoder the speed accuracy can increase

to 0.01%. In many real-life applications, the constraints are well covered by these performances. Combined with its torque fast-response, this is a major DTC advantage. A second advantage derives from the absence of sensors. Indeed, in many DTC applications, a precise closed-loop control is not critically. Another advantage derives is that DTC provides full torque at very low speed values (0.5Hz).

A Modbus [18] communication module (responsible for motor control) was integrated into the software platform to ensure the computer control. Modbus messages are being built and sent to the inverter to set the speed, start or stop the motor or to periodically read the parameters of interest (the speed, the current, the electrical and mechanical power). Modbus-related information is also displayed on the GUI (the slave address, the accessed register, the function code and the data retrieved from inverter).

Every message accesses a specific register in the inverter. Two Modbus functions are used: function 06 – writing to a single register (for start/stop and setting the speed reference) and function 03 – reading a single register (to read values for speed, current, mechanical power delivered at motor's shaft and the electrical power received from the network).

As mentioned above, the low-speed testing reveal ripples in the efficiency curve (Fig. 6). They were observed for both 500 rpm and 1 000 rpm speed reference values. The efficiency is calculated using equation 7, which suggested the ripples propagated from the mechanical power. Indeed, ripples can be found in all the data acquired from the inverter (speed, mechanical and electrical power). The acquired mechanical power delivered to the motor's shaft can be seen in Fig. 7.

The speed revealed ripples as well. As the speed reference increases, the difference between the maximum and the minimum values decreases. For example, for a speed reference of 400 rpm, the difference was $\Delta n_{400} = 411\,\text{rpm} - 390\,\text{rpm} = 21\,\text{rpm}$ while for a speed reference of 700 rpm this value was $\Delta n_{700} = 707\,\text{rpm} - 694\,\text{rpm} = 13\,\text{rpm}$.

It is important to mention that increasing the speed from 400 rpm to 700 rpm almost doubles the flow rate in the hydraulic circuit. As a result, the ripples are reduced by almost half.

$$\eta = \frac{P_u}{P_{abs}} = \frac{\rho g Q H}{P_{abs}}. \tag{7}$$

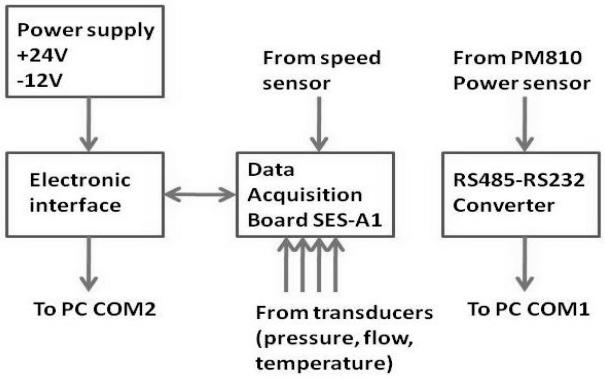

Fig. 5 – The Data Acquisition System Schematic Block Diagram.

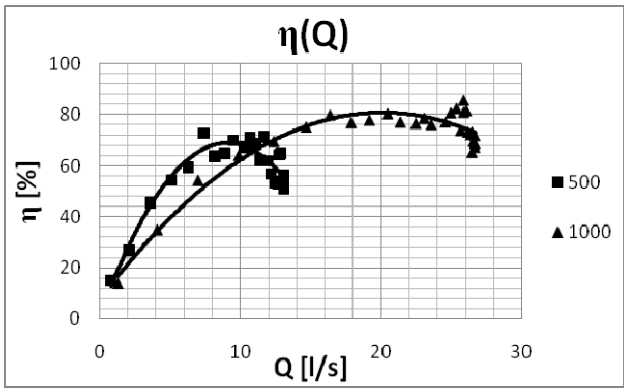

Fig. 6 – The efficiency curves for 500 and 1000 rpm speed reference.

In equation 7, Q is the flow rate, H is the head, P_{abs} is the mechanical power transferred to the pump, and ρ is the water's density. A filter is then required to eliminate the noise from the efficiency (Fig. 6). Before choosing the filter type it is important to note that the sampling frequency for the speed and the mechanical power is 1Hz. However, during testing, the acquisition frequency is much lower than 1Hz to allow the transient regimes to pass.

To be able to decide on a filter, the mechanical power spectrum was computed (Fig. 8). It is important to note that the signal's energy is almost uniformly distributed along the horizontal axis in both spectra. Consequently, a low-pass, high-pass or band-pass filter would not work in this case. Based on the above observations, a Kalman filter was chosen.

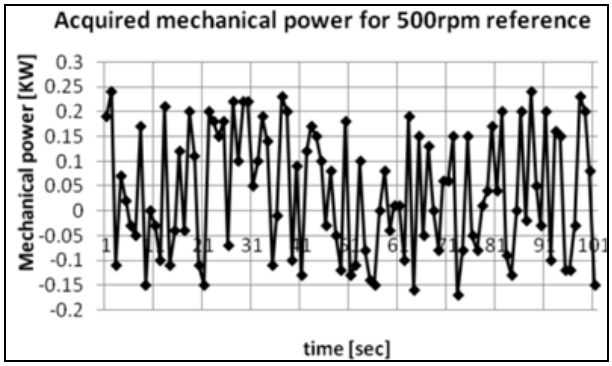

Fig 7 – The acquired mechanical power for a 500 rpm speed reference (the sampling frequency is 1Hz).

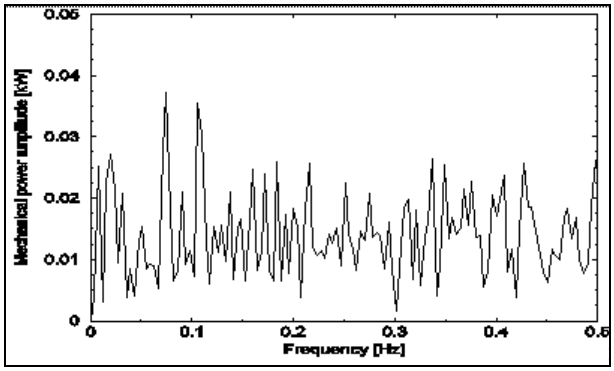

Fig 8 – The mechanical power spectrum (the sampling frequency is 1Hz).

3.2. Kalman filter's theory

The so-called "Kalman filters" were developed by Kalman in the 60 s [7]. Since then, their area of application has grown considerably. Matthies and Kanade [9] use Kalman filter-based algorithms to estimate depth from image sequences. Mohamed and Schwarz [11] use adaptive Kalman filtering for Global Positioning System.

The Kalman filter algorithm is a way to estimate the state $x \in \Re^n$ of a discrete-time controlled process governed by equation 8.

$$x_k = A \cdot x_{k-1} + B \cdot u_{k-1} + w_{k-1}, \tag{8}$$

where A is a square matrix relating the previous state x_{k-1} to the actual state x_k, u_{k-1} is the control variable and the w_{k-1} is the noise affecting the process. The measurement is written as equation 9 shows:

$$z_k = H \cdot x_k + v_k. \tag{9}$$

In equation 9 v_k is the noise affecting the measurements, and the $m \times n$ matrix H relates the measurements to the states x_k. The a priori and a posteriori estimate errors given by the measurement at iteration k are:

$$e_k^- = x_k - \hat{x}_k^-, \tag{10}$$

$$e_k = x_k - \hat{x}_k, \tag{11}$$

where $\hat{x}_k^-$ and $\hat{x}_k$ are the a priori and a posteriori estimates for iteration k. The a priori and a posteriori estimate error covariances are defined in [16] as shown below:

$$P_k^- = E[e_k^- e_k^{-T}], \tag{12}$$

$$P_k = E[e_k e_k^T]. \tag{13}$$

The state's estimation for iteration k is given by:

$$\hat{x}_k = \hat{x}_k^- + K_k \left(z_k - H \hat{x}_k^- \right), \tag{14}$$

where K_k is called the *gain*. In the literature the difference $\left(z_k - H \hat{x}_k^- \right)$ is often called the *residual*. Substituting equation 14 into equation 10 and the result into 13 and minimizing the a posteriori error covariance by taking the derivative with respect to the gain K leads to:

$$K_k = P_k^- H^T \left(H P_k^- H^T + R \right)^{-1}. \tag{15}$$

4. EXPERIMENTS AND RESULTS

For implementation, the value to be measured is considered to be constant for certain time intervals. Indeed, during testing, the acquisition interval has to be large enough to allow the transient regimes to pass. Consequently, the matrix A was set to 1. Matrix H was also set to 1. A deviation value of 0.01 was chosen for the filter's implementation. With these modifications, the filter's equations are shown in Table 1.

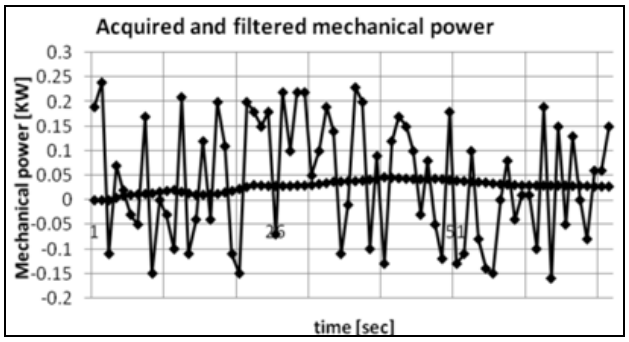

Fig. 9 – Filter's action: the acquired and the filtered mechanical power.

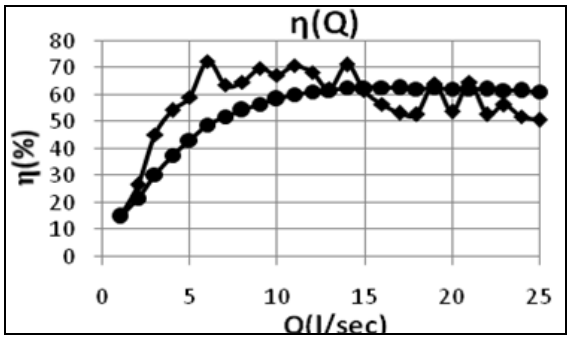

Fig. 10 – The "unfiltered" and the "noiseless" efficiency for a 500 rpm reference.

The filter's code was added to the software platform and it is currently used to filter the speed, the mechanical power, the head and the discharge. Several experiments were performed to assess the results. The filter's action on the mechanical power for a 500 rpm reference can be seen in Figure 9.

The efficiency plot calculated using filtered values for mechanical power, discharge and head versus the one obtained using the noisy values can be seen in Figure 10. As it can be seen, the filter successfully eliminates the noise from the efficiency curve.

Table 1

The Kalman filter equations

Prediction	Correction
$\hat{x}_k^- = \hat{x}_{k-1}$ $P_k^- = P_{k-1}$	$K_k = \frac{P_k^-}{P_k^- + R}$ $\hat{x}_k = \hat{x}_k^- + K_k \left(z_k - \hat{x}_k^- \right)$ $P_k = \left(1 - K_k\right) P_k^-$

5. CONCLUSIONS AND FUTURE WORK

This paper describes a method to filter the torque pulsations from a DTC inverter when actuating a speed-dependant load at small speed values. Researchers have been studied methods to eliminate torque pulsations for quite some time. However, not all DTC inverters have these control technologies implemented. Consequently, Kalman filtering is proposed to eliminate the ripples and filter the data.

This method was tested experimentally using a hardware rig built in our laboratory. The rig is actuated by a 37 KW induction motor controlled by a 45 kW DTC inverter. The filter is implemented and used to eliminate the data pulsations (noise). The results are compared against the one obtained before its filter's implementation. The proposed method preserves the "sensorless" DTC feature while successfully eliminating the ripples.

ACKNOWLEGEMENTS

This paper was supported by the project "Development and support for multidisciplinary postdoctoral programs in major technical areas of national strategy for Research – Development – Innovation" 4D-POSTDOC, contract nr. POSDRU/89/1.5/S/52603, project co-funded by the European Social Fund through Sectorial Operational Program Human Resources Development 2007-2013.

Mr. Ginga's work was partially supported by the strategic grant POSDRU/88/1.5/S/50783 (2009) of the Ministry of Labor, Family and Social Protection, Romania, co-financed by the European Social Fund – Investing in people.

Dr. Sebastian Muntean was supported by the Romanian Academy program.

REFERENCES

1. Anton, A., *In situ performance curves measurement of large pumps*, IAHR Timisoara, 10.1088/1755-1315/12/1/12090.
2. Badea A., *Schimbări climatice. Surse regenerabile de energie*, Conferința Cercetării Ştiiintifice din Învătământul Superior CNCSIS12, Masă rotundă, Energie şi dezvoltare durabilă, Bucureşti, 2010.
3. Barrio, R., Fernandez, J., Blanco, E., Parrondo, J., *Estimation of radial load in centrifugal pumps using computational fluid dynamics*, European Journal of Mechanics – B/Fluids, **30**, *3*, pp. 316–324, 2011; doi: 10.1016/j.euromechflu.2011.01.002.
4. Berteen, J., Verveckken, J., Driesen, J., 2010, *Predictive Direct Torque Control for Flux and Torque Ripple Reduction*, **57**, pp. 404–412; doi: 10.1109/TIE.2009.2033487.
5. Blaschke, F., *The principle of field orientation as applied to the new TRANSVECTOR closed loop control system for rotating field machines*, Siemens Review, **39**, *5*, pp. 217–220, 1972.
6. Depenbrock, M., *Direct self control for dynamics performance of inverter feed ac. machines*, ETZ Archiv, **7**, *7*, pp. 211–218, 1985.
7. Kalman, R. E., *A New Approach to Linear Filtering and Prediction Problems*, Transaction of the ASME—Journal of Basic Engineering, pp. 35–45, 1960.
8. Lascu, C., Boldea, I., Blaabjerg, F., *A modified Direct Torque Control (DTC) for Induction Motor Sensorless Drive*, IEEE Trans. Industrial Appl., **36**, pp. 122–130, 2000.
9. Matthies, L, Kanade, T., *Kalman Filter-based Algorithms for Estimating Depth from Image Sequences*, International Journal of Computer Vision, **3**, pp. 209–236, 1989.
10. Memardezfouli, M., Nourbakhsk, A., *Experimental investigation of slip factors in centrifugal pumps*, International Journal of Experimental Heat Transfer, Thermodynamics, and Fluid Mechanics, **33**, pp. 938–945, 2009.
11. Mohamed H., Schwarz, K.P., *Adaptive Kalman Filtering for INS/GPS*, Journal of Geodesy, **73**, pp. 193–203, 1999.
12. Savar, M., Hrvoje, K., Sutlovic, I., 2009, *Improving centrifugal pump efficiency by impeller trimming*, The International Journal on the Science and Technology of Desalting and Water Purification, **249**, pp. 654–659.
13. Sakthivel, N.,R., Sugumaran, V., Binoy, B. Nair, *Comparison of decision tree-fuzzy and rough set-fuzzy methods for fault categorization of mono-block centrifugal pump*, Mechanical Systems and Signal Processing, **24**, pp. 1887–1906, 2010.
14. Takahashi, I., Noguchi, T., *A new response and high efficiency strategy of an induction motor*, Record of IEEE IAS, Annual Meeting, pp. 495–502, 1985.
15. Vas, P., *Sensorless Vector and Direct Torque Control*, Clarendon Press, Oxford, 1998.
16. Welch, G., Bishop, G., *An Introduction to the Kalman Filter*, SIGGRAPH Chapel Hill, 2001.
17. Zidani F., Said, R., N., *Direct Torque Control of Induction Motor with Fuzzy Minimization Torque Ripple*, Journal of Electrical Engineering, **56**, *7–8*, pp. 183–188, 2005.
18. *** Modicon Modbus Reference Guide, 1996, PI-MBUS-300 Rev. J.

Received November 29, 2011